Numerical simulation of 3-D flows with a non-oscillatory central scheme on unstructured tetrahedral grids

Paul Arminjon[*†] Aziz Madrane[‡]
Amik St-Cyr[§]

CRM-2712

January 2001

[*]Dép. de math. et de stat., Université de Montréal, C.P. 6128, Succ. centre-ville, Montréal, Québec, H3C 3J7, Canada; arminjon@crm.umontreal.ca

[†]This research was supported by a grant from the National Science and Engineering Research Council of Canada, and by an FCAR grant from the Government of the Province of Québec.

[‡]Department of Math. and Stat., University of Ottawa, 585 King Edward, Ottawa, ON, K1N 6N5, Canada madrane@mathstat.uottawa.ca

[§]Dép. de math. et de stat., Université de Montréal, C.P. 6128, Succ. centre-ville, Montréal, Québec, H3C 3J7, Canada; stcyr@dms.umontreal.ca

Abstract

We present a 3D finite volume generalization of the 1-dimensional Lax-Friedrichs and Nessyahu-Tadmor schemes for hyperbolic equations on unstructured tetrahedral grids. The non-oscillatory central difference scheme of Nessyahu and Tadmor, in which the resolution of the Riemann problem at the cell interfaces is by-passed thanks to the use of the staggered Lax-Friedrichs scheme, is extended here to a two-step, three-dimensional non-oscillatory centered scheme in finite volume formulation. Piecewise linear cell interpolants using Venkatakrishnan's limiter combined with diverse techniques to estimate the gradients lead to a non-oscillatory spatial resolution of order 2. The fact that the expected second order resolution is not fully attained in 3D for nonlinear systems might be caused by the absence of grid adaptation in our calculations. Numerical results for a linear advection problem with continuous initial conditions in 3D show the accuracy and stability of the method. We also include results for the 3D Euler system (shock tube problem)

I Introduction

In earlier papers [6, 7] we presented a two-dimensional finite volume method generalizing the one-dimensi-
onal Lax-Friedrichs [12] and Nessyahu-Tadmor [14] difference schemes for hyperbolic conservation laws to unstructured triangular grids, while in [5, 2] we have also constructed a corresponding extension for 2-dimensional cartesian grids.

All these extensions to 2-dimensional problems lead to non-oscillatory, essentially second order accurate finite volume methods.

In [2, 3] we presented an extension to staggered structured three-dimensional cartesian grids of our two-dimensional finite volume method for cartesian grids. We proved that the first order three-dimensional finite volume extension of the Lax-Friedrichs scheme is monotone under an appropriate CFL condition. Some difficulties encountered in the numerical experiments led us to consider a special type of limiting function proposed by Venkatakrishnan. The method still displayed too much dissipation and requires some adjustments.

In this paper, we first present a finite volume extension of the first order accurate Lax-Friedrichs scheme to three-dimensional tetrahedral grids. We then construct the extension of our two-dimensional finite volume method to a quasi-second order accurate non-oscillatory finite volume method of "central type", for staggered unstructured tetrahedral grids, which can be viewed as a finite volume generalization of the 1-dimensional Nessyahu-Tadmor difference scheme to 3-dimensional unstructured tetrehedral grids.

II Mathematical modelling

II.1 Governing equations

Let $\Omega \subset R^3$ be the domain of interest of the flow and Γ be its boundary, we write $\Gamma = \Gamma_B \cup \Gamma_\infty \cup \Gamma_E$, where Γ_B denotes that part of the body boundary which is relevant for the computational domain. Γ_∞ is the (upwind) farfield boundary, and Γ_E is the (downwind) exit part of the boundary. The equations describing 3-dimensional compressible inviscid flows are the Euler equations, written here in their conservation form [15], given by

$$\frac{\partial U}{\partial t} + \overrightarrow{\nabla} \cdot \overrightarrow{\mathcal{F}}(U) = 0 \quad \text{where} \quad U = (\rho, \rho u, \rho v, \rho w, E)^T, \quad \overrightarrow{\mathcal{F}}(U) = (F(U), G(U), H(U))^T, \quad \text{(II.1)}$$

$\overrightarrow{\mathcal{F}}(U)$ denotes the convective flux [15], ρ is the density, $\overrightarrow{V} = (u, v, w)$ is the velocity vector, $E = \rho e = \rho\epsilon + \frac{1}{2}\rho(u^2 + v^2 + w^2)$ is the total energy per unit volume; p is the pressure of the fluid. Let A,B and C denote the Jacobian matrices $\partial F(U)/\partial U$, $\partial G(U)/\partial U$ and $\partial H(U)/\partial U$, respectively. Eq.(II.1) can be written in the nonconservative form:

$$\frac{\partial U}{\partial t} + A(U)\frac{\partial U}{\partial x} + B(U)\frac{\partial U}{\partial y} + C(U)\frac{\partial U}{\partial z} = 0 \quad \text{(II.2)}$$

II.2 Boundary conditions

The flow is assumed to be uniform at the farfield boundary Γ_∞ and we impose

$$\rho_\infty = 1, \quad \overrightarrow{V}_\infty = \begin{pmatrix} \cos\alpha\cos\beta \\ \sin\beta \\ \sin\alpha\cos\beta \end{pmatrix}, \; p_\infty = \frac{1}{\gamma M_\infty^2} \tag{II.3}$$

where α is the angle of attack, β is the yaw angle and M_∞ denotes the free-stream Mach number.On the wall boundary Γ_B, we use the following slip condition $\overrightarrow{V} \cdot \overrightarrow{n} = 0$ where $\overrightarrow{n}$ indicates the outward unit vector normal to the boundary $\Gamma_\infty \cup \Gamma_B$. Finally, for unsteady calculations, an initial flow is prescribed: $U(x,0) = U_o(x) \quad on \quad \Omega$.

III Discretization with respect to space and time

III.1 Definitions, description of the first-order method

We assume that Ω is a polyhedral bounded domain of R^3, and start from an arbitrary FEM tetrahedral grid $\mathcal{T}_h$, where h is the maximal length of the edges in $\mathcal{T}_h$. We need the following notations: T_{ij} denotes the set of all tetrahedra which share edge $[i,j]$ as a common edge. Let M denote the set of indices of all sub-tetrahedra of the original tetrahedral grid, defined by the median planes such as: iM_1GG_1,iM_1GG_3,jM_1GG_1 and jM_1GG_3 on fig. 1. Let $m(i,j,\tau,l)$ be one such index contained in M, where $\tau \in T_{ij}$ and l $(1 \leq l \leq 4)$ is the index of one of the four sub-tetrahedra sharing edge $[i,j]$ and contained in tetrahedron τ. If $l = 1,3$ then the index denotes sub-tetrahedra having node a_i in common, and, if $l = 2,4$ they share node a_j. Any such sub-tetrahedron will be noted l_k where $k \in M$. $K(i)$ is the set of nodes (vertices) which are neighbours of node a_i. Let nv be the number of vertices of $\tau \in \mathcal{T}_h$. For every vertex a_i, $1 \leq i \leq nv$ (written i for simplicity on fig. 1) of an arbitrary tetrahedron $\tau \in \mathcal{T}_h$, we define the (vertex centered) barycentric cell C_i as follows (this approach was introduced in [1]): every tetrahedron of $\mathcal{T}_h$ is subdivided in 24 sub-tetrahedra l_k by the median planes. The cell C_i is the union of the resulting sub-tetrahedra sharing a_i as a vertex $C_i = \bigcup_{j\in K(i)} \bigcup_{\tau\in T_{ij}} l_{m(i,j,\tau,\{1,3\})}$. The faces of interest associated with each sub-tetrehedron l_k $(k \in M)$ are, first, those which do not share any edge midpoint (such as M_1 in fig. 1) noted ∂l_k^1 (such as jGG_1 or jGG_3 on fig. 1), and secondly, the faces which do not contain vertex a_i in their composition, noted ∂l_k^2. The outward normals to those faces will be noted n_k for ∂l_k^1 and ν_k for ∂l_k^2 (such as, on fig. 1, M_1GG_1 or M_1GG_3). Note that we use normal vectors such that $||n_k|| = Area(\partial l_k^1)$ and $||\nu_k|| = Area(\partial l_k^2)$. The boundary ∂C_i of C_i can be constructed with ∂l_k^2 ($\partial C_i = \bigcup_{j\in K(i)} \bigcup_{\tau\in T_{ij}} \partial l^2_{m(i,j,\tau,\{1,3\})}$). As was the case in our 2-dimensional extensions, our 3-D extension also uses a dual grid, with dual cells L_{ij} associated with the edges of $\mathcal{T}_h$. The dual ("diamond") cell L_{ij} is composed by the sub-tetrahedra (defined above) sharing edge $[i,j]$ ($L_{ij} = \bigcup_{\tau\in T_{ij}} l_{m(i,j,\tau,\{1,2,3,4\})}$). Owing to the the fact that ∂l_k^1 denotes one of the facets of ∂L_{ij}, we can formulate the dependence of ∂L_{ij} on the selected faces (i.e. with superscript index 1) of the sub-tetrahedra which compose L_{ij} :

$$\partial L_{ij} = \bigcup_{\tau\in T_{ij}} \partial l^1_{m(i,j,\tau,\{1,2,3,4\})} = \bigcup_{\tau\in T_{ij}} \partial l^1_{m(i,j,\tau,\{1,3\})} \cup \partial l^1_{m(i,j,\tau,\{2,4\})} \tag{III.1}$$

Let i,j,k,l be the four nodes defining a tetrahedron τ sharing node a_i, then the cell boundary element of cell C_i, associated with τ and edge $[i,j]$ is

$$\partial C_i \cap \tau \cap L_{ij} = Triangle(M_1GG_1) \cup Triangle(M_1GG_3) = \partial l^2_{m(i,j,\tau,\{1,3\})} = \partial l^2_{m(i,j,\tau,1)} \cup \partial l^2_{m(i,j,\tau,3)} \tag{III.2}$$

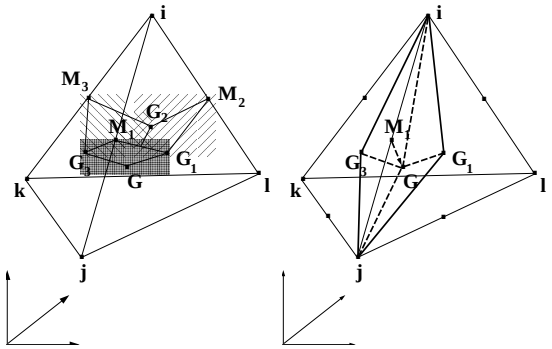

Figure 1: **Barycentric cell C_i and diamond cell L_{ij}**

Let m_{ij} denote the midpoint of edge $[i,j]$, also written as M_1 above, and let $U_i^n \cong U(a_i,t^n)$ and $U_{ij}^{n+1} \cong U(m_{ij},t^{n+1})$ denote the nodal (resp. cell average) values in the first and second grid at time $t=t^n$ and $t=t^{n+1}$, respectively (n even). The union of all the barycentric cells constitutes a partition of the computational domain Ω_h and the same holds for diamond cells:

$$\Omega_h = \bigcup_{i=1}^{nv} C_i, \quad \Omega_h = \bigcup_{k=1}^{ne} L_k$$

where nv and ne are the number of vertices and number of edges, respectively, of the original finite element triangulation $\mathcal{T}_h$. We now define the two steps of our first order accurate (staggered, Lax-Friedrichs type) finite volume method:

First time step:

In the first (and further odd) time step of our 3-dimensional finite volume scheme, we start from initial (or previously obtained) cell average values $\vec{U}_i$ for the barycentric cells of the first grid, and compute cell average values $\overrightarrow{U}_{ij}$ for the (staggered) dual cells of the second grid. This is done by integrating (II.1) on an extended control volume $L_{ij}\times[t^n,t^{n+1}]$, where L_{ij} is a (diamond) cell of the dual grid, and by assuming that $\overrightarrow{U}_{L_{ij}}(t^n+\Delta t)$ is piecewise constant on the cells of the second grid. Using (II.1) and applying the divergence theorem to the flux term, we obtain

$$\int_{t^n}^{t^{n+1}}\int_{L_{ij}} U_t d\vec{x}dt \quad + \int_{t^n}^{t^{n+1}}\int_{\partial L_{ij}} \overrightarrow{\mathcal{F}}(U)\cdot\overrightarrow{n}\; dAdt = 0 \tag{III.3}$$

Let $m(1,3)$ be equal to $m(i,j,\tau,\{1,3\})$ and $m(2,4)=m(i,j,\tau,\{2,4\})$ for simplicity, (where $m(1,3)$ is in fact dependent on i,j,τ);we obtain

$$U_{ij}^{n+1} = \frac{1}{2}(U_i^n+U_j^n) - \frac{\Delta t}{Vol(L_{ij})}\sum_{\tau\in T_{ij}}\{\overrightarrow{\mathcal{F}}(U_i^n)\cdot\overrightarrow{n}_{m(1,3)} + \overrightarrow{\mathcal{F}}(U_j^n)\cdot\overrightarrow{n}_{m(2,4)}\}$$
$$- \frac{\Delta t}{Vol(L_{ij})}\int_{\partial L_{ij}\cap\Gamma_B}\overrightarrow{\mathcal{F}}(U(\vec{x})^n)\cdot\overrightarrow{n}\,dA - \frac{\Delta t}{Vol(L_{ij})}\int_{\partial L_{ij}\cap\Gamma_\infty}\overrightarrow{\mathcal{F}}(U(\vec{x})^n)\cdot\overrightarrow{n}\,dA \tag{III.4}$$

Second time step: Starting from the known diamond cell value U_{ij}^{n+1}, we compute the barycentric cell value U_i^{n+2} $(1\le i\le nv)$ by integrating (II.1) on an extended control volume $C_i\times[t^{n+1},t^{n+2}]$, applying the divergence theorem to the flux term, and observing that

$$\partial C_i = \bigcup_{j\in K(i)}\{\partial C_i\cap\partial C_j\}\cup\{\partial C_i\cap\Gamma_B\}\cup\{\partial C_i\cap\Gamma_\infty\}.$$

We obtain

$$U_i^{n+2} = \sum_{j\in K(i)} \frac{Vol(C_i \cap L_{ij})}{Vol(C_i)} U_{ij}^{n+1} - \frac{\Delta t}{Vol(C_i)} \sum_{j\in K(i)} \sum_{\tau\in T_{ij}} \overrightarrow{\mathcal{F}}(U_i^{n+1}) \cdot \overrightarrow{\nu}_{m(1,3)}$$
$$- \frac{\Delta t}{Vol(C_i)} \int_{\partial C_i \cap \Gamma_B} \overrightarrow{\mathcal{F}}(U^{n+1}) \cdot \overrightarrow{\nu}\, dA - \frac{\Delta t}{Vol(C_i)} \int_{\partial C_i \cap \Gamma_\infty} \overrightarrow{\mathcal{F}}(U^{n+1}) \cdot \overrightarrow{\nu}\, dA \qquad \text{(III.5)}$$

III.2 High-order accurate approximations

To obtain second-order accuracy, we introduce cellwise piecewise linear interpolation (MUSCL,[16]), the derivatives of the P_1 (Galerkin) interpolation [10], Least Squares [9, 7], and the Gauss-Green formula [8]. **First step:** We integrate (II.1) on an extended control volume $L_{ij} \times [t^n, t^{n+1}]$, assuming we have obtained from the cell average values U_i^n piecewise linear reconstructions given by

$$U_h(x,y,z,t^n)_{|C_i} = \mathcal{L}_i(x,y,z,t^n) = U_i^n + (x-x_i)P_i^n + (y-y_i)Q_i^n + (z-z_i)R_i^n \qquad (x,y,z) \in C_i \qquad \text{(III.6)}$$

For the integration with respect to time, in order to ensure "nearly" second-order accuracy, we adopt a " quasi-midpoint formula" time discretization, where the convective flux is computed at the intermediate time $t^{n+\frac{1}{2}}$ (thus requiring the computation of **predicted** values $U_h(x,y,t^{n+\frac{1}{2}})$ along ∂L_{ij}), in the integration with respect to time.

Predictor (First step):

On each face of the cell L_{ij}, using the Euler equations, we define a predicted vector

$$U_{a_i,G_1,G}^{n+1/2} = U_{a_i,G_1,G}^n - \frac{\Delta t}{2}\Big\{F'(U_{a_i,G_1,G}^n)P_i^n + G'(U_{a_i,G_1,G}^n)Q_i^n + H'(U_{a_i,G_1,G}^n)R_i^n\Big\} \qquad \text{(III.7)}$$

where, using (III.6), the value of U_h^n along the face a_i, G_1, G of diamond cell L_{ij} is taken equal to

$$U_h(x,y,z,t^n) \cong U_i^n + \frac{1}{2}(x_{a_i,G_1,G} - x_i)P_i^n + \frac{1}{2}(y_{a_i,G_1,G} - y_i)Q_i^n + \frac{1}{2}(z_{a_i,G_1,G} - z_i)R_i^n \equiv U_{a_i,G_1,G}^n \qquad \text{(III.8)}$$

The corrector can now be written, using (III.7), as

Corrector (First step)

$$Vol(L_{ij})U_{ij}^{n+1} - \Big\{\int_{L_{ij}\cap C_i} \mathcal{L}(x,y,z,t^n)d\vec{x} + \int_{L_{ij}\cap C_j} \mathcal{L}(x,y,z,t^n)d\vec{x}\Big\}$$
$$+ \Delta t \sum_{\tau\in T_{ij}} \{\int_{\partial l^1_{m(i,j,\tau,\{1,3\})}} + \int_{\partial l^1_{m(i,j,\tau,\{2,4\})}}\} \overrightarrow{\mathcal{F}}(U_h^{n+\frac{1}{2}}) \cdot \overrightarrow{n}\, dA$$
$$+ \Delta t \int_{\partial L_{ij}\cap\Gamma_B} \overrightarrow{\mathcal{F}}(U_h^n) \cdot \overrightarrow{n_{ij}} dA + \Delta t \int_{\partial L_{ij}\cap\Gamma_\infty} \overrightarrow{\mathcal{F}}(U_h^n) \cdot \overrightarrow{n_{ij}} dA = 0 \qquad \text{where} \qquad \text{(III.9)}$$

$$\int_{L_{ij}\cap C_i} \mathcal{L}(x,y,z,t^n)d\vec{x} = \sum_{\tau\in T_{ij}} Vol(l_{m(1,3)})\mathcal{L}(x_{\mathcal{G}_{m(1,3)}}, y_{\mathcal{G}_{m(1,3)}}, z_{\mathcal{G}_{m(1,3)}}, t^n) \qquad \text{(III.10)}$$

where $\mathcal{G}_{m(1,3)}$ is the centroid of sub-tetrahedron $l_{m(1,3)}$. Note that from the coding viewpoint there is a simplification since the two sub-tetrahedra $(1,3)$ also form a convex polyhedron the barycenter of which can be calculated, and the last integral can be simplified.

Second step

To obtain the second step of the time discretization, we integrate (II.1) on the cell $C_i \times [t^{n+1}, t^{n+2}]$, assuming we have obtained, from the diamond cell average values U_{ij}^{n+1} computed in the first time step, piecewise linear reconstructions, given by

$$U_h(x,y,z,t^{n+1})_{|_{L_{ij}}} = \mathcal{L}_{ij}(x,y,z,t^{n+1}) = U_{ij}^{n+1} + (x-x_{ij})P_{ij}^{n+1} + (y-y_{ij})Q_{ij}^{n+1} + (z-z_{ij})R_{ij}^{n+1} \tag{III.11}$$

Proceeding as for the first step, we obtain

Predictor (second step)

$$U_{G,G_1,M_1,G_3}^{n+\frac{3}{2}} = U_{G,G_1,M_1,G_3}^{n+1} - \frac{\Delta t}{2}\Big\{F'(U_{G,G_1,M_1,G_3}^{n+1})P_{ij}^{n+1} + G'(U_{G,G_1,M_1,G_3}^{n+1})Q_{ij}^{n+1} + H'(U_{G,G_1,M_1,G_3}^{n+1})R_{ij}^{n+1}\Big\} \tag{III.12}$$

where

$$U_h(x,y,z,t^{n+1}) \cong U_{ij}^{n+1} + \frac{1}{2}(x_G - x_{M_1})P_{ij}^{n+1} + \frac{1}{2}(y_G - y_{M_1})Q_{ij}^{n+1} + \frac{1}{2}(z_G - z_{M_1})R_{ij}^{n+1} \equiv U_{G,G_1,M_1,G_3}^{n+1} \tag{III.13}$$

defines an approximation of the value of U on the boundary element $[G, G_1, M_1, G_3]$ of cell C_i.

Corrector (second step)

$$\begin{aligned} &Vol(C_i)U_i^{n+2} - \sum_{j\in K(i)} \int_{C_i\cap L_{ij}} \mathcal{L}_{ij}(x,y,z,t^{n+1})d\vec{x} + \Delta t \sum_{j\in K(i)} \sum_{\tau\in T_{ij}} \int_{\partial l^2_{m(i,j,\tau,\{1,3\})}} \overrightarrow{\mathcal{F}}(U(x,y,z,t^{n+3/2}))\cdot\overrightarrow{\nu}\,dA \\ &+ \Delta t \int_{\partial C_i\cap\Gamma_B} \overrightarrow{\mathcal{F}}(U_h^{n+1})\cdot\overrightarrow{\nu}\,dA + \Delta t \int_{\partial C_i\cap\Gamma_\infty} \overrightarrow{\mathcal{F}}(U_h^{n+1})\cdot\overrightarrow{\nu}\,dA = 0 \end{aligned} \tag{III.14}$$

where

$$\int_{C_i\cap L_{ij}} \mathcal{L}_{ij}(x,y,z,t^{n+1})d\vec{x} = \sum_{j\in K(i)} \sum_{\tau\in T_{ij}} \{Vol(l_{m(i,j,\tau,1,3)})\mathcal{L}(x_{\mathcal{G}_m(i,j,\tau,1,3)}, y_{\mathcal{G}_m(i,j,\tau,1,3)}, z_{\mathcal{G}_m(i,j,\tau,1,3)}, t^{n+1})\} \tag{III.15}$$

is computed according to III.10 with the respective barycenters of the sub-tetrahedra (again, a simplification is possible).

III.2.1 Approximation of the slopes and limitation

In order to compute the gradient (P_i^n, Q_i^n, R_i^n) of the piecewise linear interpolant $L(x,y,z,t^n)$ for the cell C_i, we use the P_1 (Galerkin) interpolation [10], Least Squares [9, 7] and Gauss-Green [8]. For the limitation we use several procedures, see [16]. Numerical experiments have led us to choose the Gauss-Green formula for the gradients used in the reconstruction for the cells C_i and a least squares weighted procedure for the cells L_{ij}.

III.2.2 Treatment of the boundary conditions

To implement the boundary conditions,

$$\int_{\partial C_i \cap \Gamma_B} \overrightarrow{\mathcal{F}}(U_h^{n+1}) \cdot \overrightarrow{\nu_i} dA = \int_{\partial C_i \cap \Gamma_B} \begin{pmatrix} 0 \\ p\nu_x \\ p\nu_y \\ p\nu_z \\ 0 \end{pmatrix}^{n+1} dA, \tag{III.16}$$

we use the following approximation

$$\int_{\partial C_i \cap \Gamma_\infty} \overrightarrow{\mathcal{F}}(U_h^{n+1}) \cdot \overrightarrow{\nu_i} dA = \mathcal{A}^+(U_i, \overrightarrow{\nu}_{i\infty}) \cdot U_i + \mathcal{A}^-(U_i, \overrightarrow{\nu}_{i\infty}) \cdot U_\infty \tag{III.17}$$

where $\mathcal{A}(U_i, \overrightarrow{\nu}_{i\infty}) = \overrightarrow{\mathcal{F}'}(U_i) \cdot \int_{\partial C_i \cap \Gamma_\infty} \overrightarrow{\nu_i} dA$ and where $\mathcal{A}^+$ and $\mathcal{A}^-$ are derived from the diagonalisation of $\mathcal{A}$:

$$\mathcal{A} = P\mathcal{D}P^{-1},\ \mathcal{D} \text{ diagonal}\ ;\ \mathcal{A}^+ = P\mathcal{D}^+P^{-1}\ ;\ \mathcal{A}^- = P\mathcal{D}^-P^{-1}$$

III.2.3 Stability

We refer to [13] for a stability study of linear multidimensional advection models that is also valid in the 3-D case. For the second time step:

$$\Delta t_i = \frac{Vol(C_i)}{\lambda^i_{max} \int_{\partial C_i} dA} \quad \text{where} \quad \lambda^i_{max} = \max(\lambda_i, \max_{j\ neighbour\ of\ i} \lambda_j) \quad \text{and} \quad \lambda_i = ||\overrightarrow{V}_i|| + c_i$$

and $\overrightarrow{V}_i$, c_i refer to the values in the cell C_i of the velocity vector and sound speed, respectively. We then choose the minimum Δt_i for all indices i $(1 \leq i \leq nv)$ $\Delta t = \min_{1 \leq i \leq nv} \{\Delta t_i\}$ with a similar time step definition for the first (odd) step $(t^n \rightarrow t^{n+1})$.

IV Numerical experiments

IV.1 Linear advection problem

First, to confirm the spatial accuracy of the scheme, a simple advection test is performed on a smooth initial distribution. The distribution is advected near the boundary of the cube $[0,1]^3$ and compared with the exact solution of the following problem:

$$u_t + u_x + u_y + u_z = 0 \tag{IV.1}$$

$$u(x,y,z,t=0) = f(r^2) = \begin{cases} \cos(4\pi r^2) & \text{if } r^2 \leq 1/8 \\ 0 & \text{otherwise} \end{cases}$$

where $r^2 = (x-1/2)^2 + (y-1/2)^2 + (z-1/2)^2$. Table 1 shows the L_1-error and accuracy order; the limiting function used was the one proposed by Venkatakrishnan [17].

Diameter	Nodes	L^1-error	Order
0.134057	4095	0.0487568	
0.123977	5733	0.0416913	2.0027

Table 1: L^1 - error and accuracy order, continuous problem

IV.2 Shock tube problem

To illustrate the accuracy of our scheme, we present numerical results for a 3-D extension of the shock tube problem introduced by Sod . In this problem, an initial discontinuity in the thermodynamical state of the gas breaks into a shock wave followed by a contact discontinuity and a rarefaction wave. Finite element meshes with 909,1809 and 3609 nodes are used and the initial conditions at $t = 0$ are specified by the data

$$\begin{cases} \rho = 1; u = 0; v = 0; w = 0; p = 1.0 & x \in [0, 1/2] \\ \rho = 0.125; u = 0; v = 0; w = 0; p = 0.1 & x \in [1/2, 1] \end{cases} \tag{IV.2}$$

The profiles of density, velocity, pressure and temperature are compared with the analytical solution at $t = 0.16$. The numerical solution of the 3-dimensional shock tube problem is clearly much more

h	Nodes	L^2 ρ	Order	L^2 V_z	Order	L^2 P	Order
0.01	909	2.898e-05		9.982e-05		2.778e-05	
0.005	1809	1.555e-05	0.898	6.399e-05	0.641	1.196e-05	1.216

Table 2: L^2 - error and accuracy order, Sod's problem

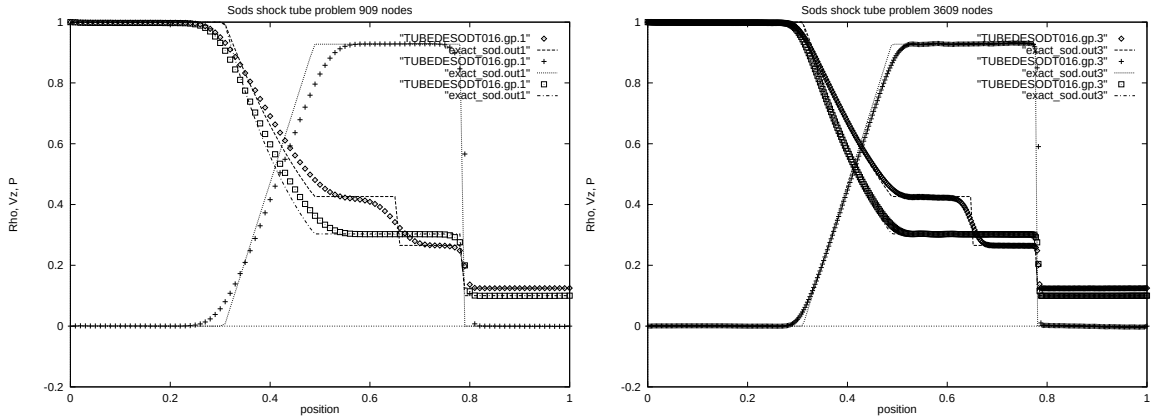

Figure 2: Sod's shock tube problem with 909 and 3609 gridpoints

likely to suffer from excessive numerical dissipation than its 1-dimensional analogue see e. g. [11]. In our case, see table 2 and Fig. 2, this dissipation might be due to the fact that the tetrahedra are fairly stretched (the aspect ratio is more than 1 : 25). This creates an additional difficulty for the capture of the shock and particularly of the contact discontinuity. Mesh adaptation, which was not available to us, would certainly bring a decisive improvement, as was observed in our 2-dimensional experiments [7].

V Conclusion

In this paper we have presented a new construction of three-dimensional finite volume methods for inviscid flows using staggered unstructured tetrahedral grids. The first and second-order methods can be considered as finite volume generalizations of the Lax-Friedrichs and Nessyahu-Tadmor 1-dimensional difference schemes, respectively. Actual calculations have been restricted to the higher-order method, as the first-order Lax-Friedrichs-type method, in three dimensions, proved to be even more dissipative than in one dimension. Nevertheless the quality of the results does not fully meet original expectations, based on the very high quality obtained with our method for 2-dimensional flows [7], where we were using grid adaptation. We could probably attribute the excessive dissipation in part to the grids, which have a relatively small number of nodes, a high aspect ratio, and have not benefited from the improvements brought about by grid adaptation. We are currently working on this problem.

References

[1] Angrand F., Boulard V., Dervieux A., Periaux J., Vijayasundaram G., (1984), *Triangular finite element methods for the Euler equations*, 6th Int. Conf. on Comp. Meth. in Appl. Sciences and Engineering, Glowinski R., Lions J.L., Eds., North Holland .

[2] P. Arminjon, A. Madrane and A. St-Cyr (1999), *New Lax-Friedrichs-type finite volume schemes on 2 and 3D cartesian staggered grids*, 7th annual conference of the CFD Society of Canada, May 30 to June 1, 1999, Halifax, J. Militzer, editor, pp.(3-3)-(3-10).

[3] P. Arminjon, A. Madrane, A. St-Cyr,*New 2 and 3-dimensional non-oscillatory central finite volume methods for staggered cartesian grids*, to appear in SIAM J. on Scientific Computing.

[4] P. Arminjon, A. Madrane, A. St-Cyr *Numerical simulation of 3-D flows with a non-oscillatory central scheme on unstructured tetrahedral grids*, Res. Report No. 2674, Centre de Recherche Mathématiques, Univ. de Montréal, Canada.

[5] P. Arminjon, D. Stanescu and M. C. Viallon, (1995), *A two-dimensional finite volume extension of the Lax-Friedrichs and Nessyahu-Tadmor schemes for compressible flows*, Proc.of the 6th. Int. Symp. on Comp. Fluid Dynamics, Lake Tahoe (Nevada) September 4-8, 1995, M.Hafez and K. Oshima, editors, Vol. IV, pp. 7-14.

[6] P. Arminjon and M. C. Viallon, (1995), *Généralisation du schéma de Nessayahu-Tadmor pour une équation hyperbolique à deux dimensions d'espace*, C.R. Acad. Sci. Paris, t.320, série I, January 1995, pp. 85-88.

[7] P. Arminjon, M.C. Viallon and A. Madrane, (1994), *A Finite Volume Extension of the Lax-Friedrichs and Nessyahu-Tadmor Schemes for Conservation Laws on Unstructured Grids*, revised version with numerical applications, Int. J. of Comp. Fluid Dynamics (1997), Vol. 9, No. 1, 1-22.

[8] T. J.Barth and D. C.Jespersen, (1989), *The design and application of upwind schemes on unstructured meshes*,AIAA Paper No. 89-0366, 27th Aerospace sciences meeting, January 9-12, 1989, Reno, Nevada.

[9] Champier,S., (1992), *Convergence de schémas numériques type Volumes Finis pour la résolution d'équations hyperboliques*, Ph. D. dissertation, Univ. de St-Étienne, France.

[10] Fezoui,L., Lanteri,S. , Larrouturou,B. and Olivier,C., (1989), *Résolution Numérique des Équations de Navier-Stokes pour un Fluide Compressible en Maillage triangulaire*, INRIA Res. Rep. No. 1033, Inst. National de Rech. en Informatique et Automatique, Rocquencourt, 78153 Le Chesnay, France.

[11] Fezoui,L., Steve, H. and Selmin, V. (1988) *Simulation numérique d'écoulements compressibles 3-D par un schéma décentré en maillage non-structuré*, INRIA Res. Rep. No. 0825, Institut National de Recherche en Informatique et Automatique, Roquencourt, 78153 Le Chesnay, France.

[12] P.D. Lax, (1954), *Weak solutions of nonlinear hyperbolic equations and their numerical computation*, Comm. Pure and Applied Math.7, pp. 159-193.

[13] A. Madrane, (1998), *Constructions of new finite volume/finite element methods for transonic/supersonic compressible flows*, Ph. D. dissertation, Université de Montréal, Département de Mathématiques et Statistique.

[14] H. Nessyahu and E. Tadmor, (1990), *Non-oscillatory central differencing for hyperbolic conservation laws*, J. Comp. Phys., 87, No. 2, pp. 408–463.

[15] Peyret, R. and Taylor, T.-D., (1983), *Computational Methods for Fluid Flow,* Springer-Verlag,New-York, Heidelberg, Berlin.

[16] B. van Leer, (1979), *Towards the ultimate conservative difference scheme V. A Second-Order Sequel to Godunov's Method*, J.Comp.Physics, 32, pp. 101-136.

[17] V. Venkatakrishnan, (1995), *Convergence to Steady State Solutions of the Euler Equations on Unstructured Grids with Limiters*, J. Comp. Phys. 118, pp. 120-130.